Journal of Molecular Catalysis A: Chemical 426 (2017) 350–356

Contents lists available at ScienceDirect

Journal of Molecular Catalysis A: Chemical

journal homepage: www.elsevier.com/locate/molcata

Catalytic C-H oxidations by nonheme mononuclear Fe(II) complexes of two pentadentate ligands: Evidence for an Fe(IV) oxo intermediate

Mainak Mitra[a], Hassan Nimir[b], David A. Hrovat[c,e], Albert A. Shteinman[d], Michael G. Richmond[e], Miquel Costas[f], Ebbe Nordlander[a,*]

[a] Chemical Physics, Department of Chemistry, Lund University, Box 124, SE-221 00, Lund, Sweden
[b] Department of Chemistry and Earth Sciences, College of Arts and Sciences, Qatar University, P.O. Box 2713, Doha, Qatar
[c] Center for Advanced Scientific Computing and Modeling, University of North Texas, Denton, TX 76203, United States
[d] Institute of Problems of Chemical Physics, 142432, Chernogolovka, Moscow district, Russian Federation
[e] Department of Chemistry, University of North Texas, Denton, TX 76203, United States
[f] QBIS, Department of Chemistry, University de Girona, Campus Montilivi, E-17017, Girona, Spain

ARTICLE INFO

Article history:
Received 7 September 2016
Received in revised form 6 October 2016
Accepted 7 October 2016
Available online 11 October 2016

Dedicated to Dr. Georgiy B. Shul'pin in recognition of his outstanding contributions to studies of C—H bond activation and molecular oxidation reactions

Keywords:
Nonheme
Iron
Oxidation catalysis
Kinetic isotope effect
H-atom abstraction

ABSTRACT

The oxidation reactions of alkanes with hydrogen peroxide and peracids (peracetic acid (PAA) and *m*-chloroperoxybenzoic acid (mCPBA)) catalysed by two Fe(II) complexes of pentadentate {N_5}-donor ligands have been investigated. Kinetic isotope effect experiments and the use of other mechanistic probes have also been performed. While the total yields of oxidized products are similar regardless of oxidant (e.g. 30–39% for oxidation of cyclohexane), the observed alcohol/ketone ratios and kinetic isotope effects differ significantly with different oxidants. Catalytic reactions in H_2O_2 medium are consistent with the involvement of hydroxyl radicals in the C—H bond cleavage step, and resultant low kinetic isotope effect values. On the other hand, catalytic reactions performed using peracid media indicate the involvement of an oxidant different from the hydroxyl radical. For these reactions, the kinetic isotope effect values are relatively high (within a range of 4.2–5.1) and the C3/C2 selectivity parameters in adamantane oxidation are greater than 11, thereby excluding the presence of hydroxyl radicals in the C—H bond cleavage step. A low spin Fe(III)-OOH species has been detected in the H_2O_2-based catalytic system by UV/Vis, mass spectrometry and EPR spectroscopy, while an Fe(IV)-oxo species is postulated to be the active oxidant in the peracid-based catalytic systems. Computational studies on the C—H oxidation mechanism reveal that while the hydroxyl radical is mainly responsible for the H-atom abstraction in the H_2O_2-based catalytic system, it is the Fe(IV)-oxo species that abstracts the H-atom from the substrate in the peracid-based catalytic systems, in agreement with the experimental observations.

1. Introduction

The selective functionalization of organic substrate molecules remains a great challenge in catalysis research [1]. For decades, considerable efforts have been made to develop robust and selective homogeneous oxidation catalysts based on transition metals [2]. Nature employs a number of heme and nonheme iron enzymes to carry out analogous vital biological transformations, involving oxidation of substrates that use dioxygen as the ultimate oxidant [3–5]. These metalloenzymes show high regio- and stereoselectivity and operate under mild conditions [4]. Examples of such enzymes include soluble methane monooxygenases [6] and Rieske oxygenases [4,7] (Fig. 1).

Inspired by Nature, a wide range of mononuclear nonheme iron complexes have been synthesized and investigated as catalysts for the oxidation of alkanes and alkenes, using hydrogen peroxide, peracids, or dioxygen as an external oxidant [8–11]. Amongst these complexes, mononuclear Fe(II) catalysts bearing tetradentate N4-donor ligands, such as TPA [12], BPMEN [13], BQEN [10b], *S,S*-PDP [14], ^{Me2}PyTACN, [15] ^{Me2,MeBzIm}TACN [16], deserve special mention (Fig. 2). Such Fe(II) complexes exhibit excellent catalytic efficiencies in hydrocarbon oxidation reactions with high stereoretention and C—H bond selectivity. An important structural feature regarding the above-mentioned catalysts is that the Fe(II) ion has two *cis*-coordinated labile sites, which is considered to be a prerequisite for efficient catalytic oxidation.

* Corresponding author.
E-mail address: Ebbe.Nordlander@chemphys.lu.se (E. Nordlander).

http://dx.doi.org/10.1016/j.molcata.2016.10.010
1381-1169/

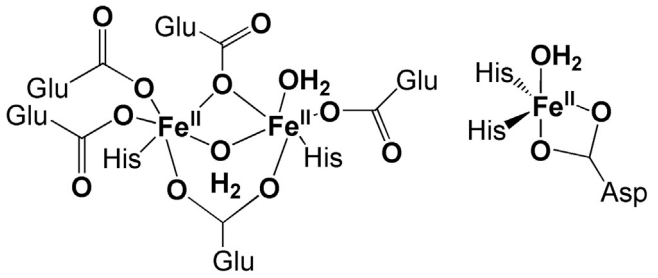

Fig. 1. The active site structures of soluble methane monooxygenase (reduced form, left), and a Rieske oxygenase (right).

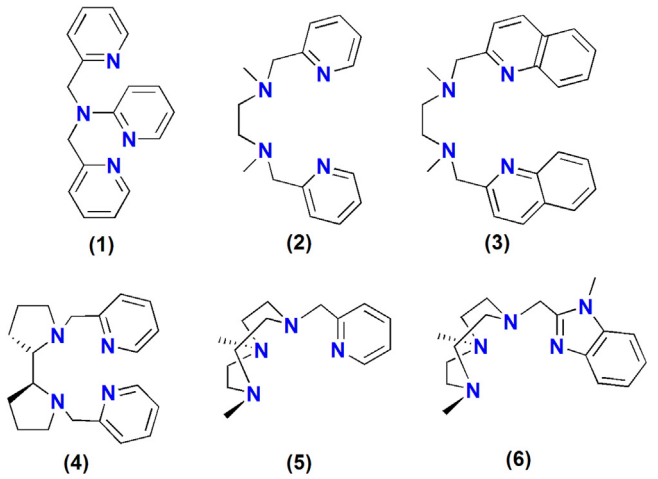

Fig. 2. The structures of the ligands, TPA (**1**), BPMEN (**2**), BQEN (**3**), *S*,*S*-PDP (**4**), ^{Me2}PyTACN (**5**) and ^{Me2,MeBzIm}TACN (**6**).

On the other hand, activated bleomycin, a biomolecule and potential antitumor drug that effects the oxidative cleavage of DNA and also the oxidation of hydrocarbons [17], contains a low spin Fe(III)-hydroperoxo unit surrounded by five nitrogen donors [18]. Therefore, oxygen activation and hydrocarbon oxidation by mononuclear Fe(II) complexes containing pentadentate ligands with one labile coordination site have been studied extensively during the last two decades [19–27]. Reactions with suitable oxidants, e.g. O_2, H_2O_2, PhIO, give rise to Fe(III)-OOH or Fe(IV)=O intermediates that have been characterized by various spectroscopic techniques [28–30]. In contrast to the ferrous complexes of tetradentate ligands that have been discussed above, Fe(II) complexes of pentadentate ligands can form high valent Fe(IV)=O intermediates that possess relatively high thermal stability, permitting thorough investigations of such high-valent intermediates in oxidative transformation reactions. In this context, the pentadentate ligand N4Py and its Fe(II)-complex are noteworthy [19]. Both $[Fe^{III}(OOH)(N4Py)]^{2+}$ [19a,28] and $[Fe^{IV}(O)(N4Py)]^{2+}$ [29] have been synthesized from the Fe(II) precursor complex and characterized. The catalytic activities of the Fe(II) complex of N4Py have been studied [20] and the involvement of $[Fe^{III}(OOH)(N4Py)]^{2+}$ and $[Fe^{IV}(O)(N4Py)]^{2+}$ as possible active oxidants during catalysis has been established both experimentally and theoretically [20,27,30,31].

We have previously demonstrated that successive replacement of pyridyl substituents of the ligand N4Py by (*N*-methyl)benzimidazolyl moieties results in an increase in the rates of hydrogen atom abstraction reactions and oxo-transfer reactions by the Fe(IV)-oxo complexes $[Fe^{IV}(O)(L^1)]^{2+}$ and $[Fe^{IV}(O)(L^2)]^{2+}$ (L^1 = [*N*-(1-methyl-2-benzimidazolyl)methyl-*N*-(2-pyridyl)methyl-*N*-(bis-2-pyridylmethyl)amine]; L^2 = [*N*-bis(1-methyl-2-benzimidazolyl)methyl-*N*-(bis-2-pyridylmethyl)amine]; Fig. 3) [32]. Here

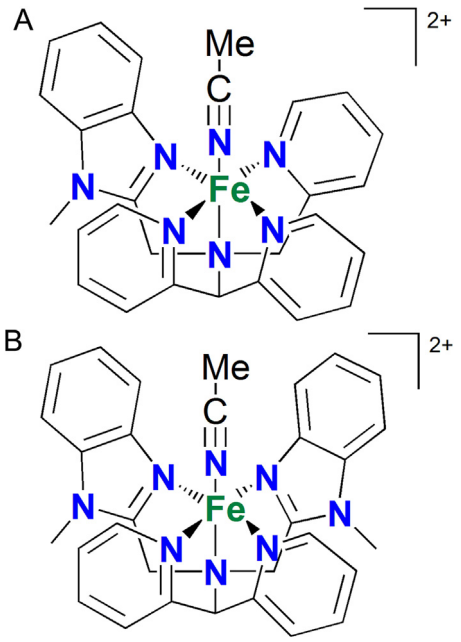

Fig. 3. The structures of the Fe(II)-complexes, $[Fe(L^1)(CH_3CN)]^{2+}$ ($\mathbf{1}^{2+}$) (top) and $[Fe(L^2)(CH_3CN)]^{2+}$ ($\mathbf{2}^{2+}$) (bottom).

we report the oxidation of various hydrocarbons by H_2O_2 or peracids, using the complexes $[Fe^{II}(L^1)CH_3CN)]^{2+}$ ($L = L^1$, L^2) as catalyst precursors. Spectroscopic studies of possible reactive intermediates operating during catalysis are also described. A detailed theoretical study on the reaction mechanisms involving H_2O_2 and peracids is described.

2. Results and discussion

The catalytic activities of the two ferrous complexes $[Fe^{II}(L^1)(CH_3CN)](ClO_4)_2$ (**1**) and $[Fe^{II}(L^2)(CH_3CN)](ClO_4)_2$ (**2**) (Fig. 3) were studied in oxidation of different alkanes, utilizing hydrogen peroxide, peracetic acid (PAA) or *m*-chloroperoxybenzoic acid (mCPBA) as co-oxidants. The oxidation reactions were carried out under standard catalytic conditions (1:100:1000 ratio for catalyst:oxidant:substrate) in acetonitrile at room temperature, and the results were compared to those for $[Fe^{II}(N4Py)(CH_3CN)](ClO_4)_2$. The oxidant was added using a syringe pump and a large excess of substrate was used to minimize over-oxidation of the products.

Complex **1** together with H_2O_2 (100 equiv.) oxidizes cyclohexane, and a turnover number (TON) of 21.1 for cyclohexanol and 18.0 for cyclohexanone was obtained with an overall yield of 39% (based on oxidant). Under similar conditions, for complex **2**, a TON of 17.4 for cyclohexanol and 14.7 for cyclohexanone was obtained with an overall yield of 32% (Table 1). The alcohol/ketone (A/K) ratio was found to be low (1.2) in both cases, and may be explained by considering the possible involvement of freely diffusing carbon-centered radicals that are trapped by molecular oxygen, followed by a Rus-

Table 1
Catalytic oxidation of cyclohexane carried out by complexes **1** and **2** with H_2O_2[a].

Complex	TON of A[b]	TON of K[c]	Yield (%)	A/K	KIE[d]
1	21.1	18	39	1.2	1.5
2	17.4	14.7	32	1.2	1.7

[a] Reaction conditions: see Experimental section.
[b] Cyclohexanol.
[c] Cyclohexanone.
[d] Kinetic isotope effect was determined for the formation of cyclohexanol from a competitive reaction of a (1:1) mixture of cyclohexane and cyclohexane-d_{12}.

Table 2
Catalytic oxidation of cyclohexane carried out by complexes **1** and **2** with PAA and mCPBA[a].

Complex	Oxidant	TON of A[b]	TON of K[c]	Yield (%)	A/K	KIE[d]
1	PAA	3.8	1.3	5.1	3.0	5.0
2	PAA	5.2	4.0	9.2	1.3	5.1
1	mCPBA	23	6.9	30	3.3	4.2
2	mCPBA	22.3	10.2	32.5	2.2	4.5

[a] Reaction conditions: see Experimental section.
[b] Cyclohexanol.
[c] Cyclohexanone.
[d] Kinetic isotope effect was determined for the formation of cyclohexanol from a competitive reaction of a (1:1) mixture of cyclohexane and cyclohexane-d_{12}.

sell termination step [9]. Addition of 50 mol% (w.r.t. the oxidant, H_2O_2) of acetic acid does not lead to any significant improvement of the overall yield or A/K ratio in cyclohexane oxidation. The kinetic isotope effect (KIE) was determined for the formation of cyclohexanol in competition experiments between cyclohexane and its d_{12} isotopomer. The KIE values obtained for complexes **1** and **2** were 1.45 and 1.7, respectively. These low KIE values are consistent with the involvement of hydroxyl radicals in the rate-determining step of C—H bond cleavage [9]. When cyclooctane was employed as the substrate, both cyclooctanol and cyclooctanone were formed. Complex **1** together with H_2O_2 (50 eq.) produced cyclooctanol with a TON of 3.7 and cyclooctanone with a TON of 14 and an overall yield of 36%, while complex **2** together with H_2O_2 (100 eq.) produced cyclooctanol with a TON of 6.6 and cyclooctanone with a TON of 24.7 and an overall yield of 31%.

The oxidation of adamantane by **1**/**2** was examined to probe the nature of the H-abstracting species, on the basis of the tertiary to secondary (C3/C2) C—H bond selectivity. The C3/C2 parameters in this reaction were small (the normalized C3/C2 ratio obtained was 3.6 for **1** and 4.5 for **2**), and thus consistent with the formation of a highly reactive but poorly selective species. Finally, complexes **1**/**2** together with H_2O_2 oxidized *cis*-1,2-dimethylcyclohexane (*cis*-DMCH) to both *cis*- and *trans*-1,2-dimethylcyclohexanol. The reaction took place without retention of configuration. Overall, the reactivity patterns that arise from the oxidation of these mechanistic probes are consistent with Fenton type activation of H_2O_2 to generate hydroxyl radicals that then attack the substrate, generating freely diffusing carbon centered radicals [9].

The behaviour of **1**/H_2O_2 with olefins also supports the mechanistic conclusions derived from the alkane oxidation reactions by H_2O_2. Styrene was converted mainly into benzaldehyde (yield 41%) and only a small amount of styrene epoxide (yield 3%) was obtained. Cyclohexene oxidation afforded the corresponding allylic alcohol and ketone as the major product and a minor amount of cyclohexene epoxide was formed.

Analogous reactions were carried out using peracids. On using peracetic acid (PAA), both the conversion and turnover numbers diminished. Complex **1** gave an overall conversion of 5% with a TON of 3.8 for cyclohexanol (A) and 1.3 for cyclohexanone (K) (A/K = 3), while complex **2** gave an overall conversion of 9% with a TON of 5.2 for cyclohexanol and 4.0 for cyclohexanone (A/K = 1.3) (Table 2). On the other hand, mCPBA exhibited a catalytic efficiency analogous to H_2O_2. Complex **1** produced an overall yield of 30%, TON for A = 23, TON for K = 6.9, and complex **2** produced an overall yield 32.5%, TON for A = 22.3, TON for K = 10.2 (Table 2). The A/K ratios were slightly increased in favour of the alcohol product (complex **1**, A/K ~ 3; complex **2**, A/K ~ 2). The KIE values estimated in the competitive oxidation of cyclohexane and its perdeuterated analogue were found to be higher than with H_2O_2 for both complexes (Table 2). On the basis of the improved A/K ratio and comparatively high(er) KIE values, significant participation of hydroxyl radicals in the peracid-based oxidation reactions may be excluded.

Table 3
Comparison of catalytic efficiencies between complexes **1**, **2** and $[Fe^{II}(N4Py)(CH_3CN)](ClO_4)_2$ (**3**)[a] for cyclohexane oxidation.

Complex	Oxidant	Total Yield (%)[b]	A/K[c]	KIE[d]
1	H_2O_2[e]	39	1.2	1.5
2	H_2O_2[e]	32	1.2	1.7
3[f]	H_2O_2[e]	30.5	1.0	1.5
1	mCPBA[g]	30	3.3	4.2
2	mCPBA[g]	32	2.2	4.5
3[h]	mCPBA[g]	33	5.6	4.5

[a] Reaction conditions: 1:100:1000 for cat:oxidant:sub in CH_3CN at RT.
[b] Total yield of cyclohexanol and cyclohexanone.
[c] Moles of cyclohexanol/moles of cyclohexanone.
[d] The kinetic isotope effect was determined for the formation of cyclohexanol from a competitive reaction of a (1:1) mixture of cyclohexane and cyclohexane-d_{12}.
[e] Under air.
[f] Ref. [20].
[g] Under inert atm.
[h] Ref. [27].

Furthermore, selectivity probes indicated that oxidations with peracids involve species more selective than those involved with H_2O_2 (*vide supra*). For example, in the oxidation of adamantane by **1**/peracid, the C3/C2 parameters (oxidation at tertiary C—H bonds vs. oxidation at secondary C—H bonds) were found to be significantly higher (the normalized C3/C2 ratio obtained for **1** was 15.8 with PAA and 11.4 with mCPBA). For complex **2**, the normalized C3/C2 parameters were 15.0 (with PAA) and 12.3 (with mCPBA). More interestingly, the C3/C2 selectivity/ratio in the oxidation of *cis*-DMCH by **1** was around 1 with H_2O_2, but this selectivity was found be approximately 12 with PAA/mCPBA. Since tertiary C—H bonds are weaker than secondary C—H bonds, the observation of large C3/C2 is indicative of the implication of an oxidant that is highly sensitive to the strength of the C—H bond. Consequently, reactions with peracids occur via species much more selective than those implicated in H_2O_2 reactions, which are likely to be the hydroxyl radical. However, the oxidation of *cis*-DMCH occurs without stereoretention, irrespective of the oxidant employed, implicating the presence of long-lived carbon centered radicals.

The catalytic efficiencies of complexes **1** and **2** are comparable to those of $[Fe^{II}(N4Py)(CH_3CN)](ClO_4)_2$ [20,27] in oxidations utilizing both H_2O_2 and peracids. For example, both complex **1** and complex **2** convert cyclohexane into cyclohexanol and cyclohexanone with overall yields of 39 and 32%, respectively (*vide supra*), while the value for $[Fe^{II}(N4Py)(CH_3CN)](ClO_4)_2$ was 30% (Table 3). The A/K ratio lies in the range 1–2 for all three (pre-)catalysts. The low KIE values suggest significant participation of hydroxyl radicals in the rate-determining step when H_2O_2 is used as oxidant. When mCPBA was employed as co-oxidant, the yields were found to be similar (30% for complex **1**, 32.5% for complex **2** and 33% for $[Fe^{II}(N4Py)(CH_3CN)](ClO_4)_2$) to those obtained in the analogous H_2O_2 systems, but the A/K ratio slightly improved in the mCPBA system (Table 3). The KIE values for all three complexes were high (in the range 4–5, Table 3) excluding significant participation of hydroxyl radicals.

3. Study of reaction intermediates formed during catalysis

UV/Vis spectrophotometry was used to identify possible reactive intermediates involved in the oxidation processes effected by the complex $[Fe^{II}(L^1)(CH_3CN)](CF_3SO_3)_2$ ($\mathbf{1}^{OTf}$) (*cf.* Experimental Section for synthesis) with H_2O_2 or peracids. The addition of excess H_2O_2 to complex $\mathbf{1}^{OTf}$ (0.5 mM) in acetonitrile at room temperature led to the formation of a transient purple species, having a characteristic absorbance maximum at λ_{max} = 535 nm ($\varepsilon \approx 640\ M^{-1}\ cm^{-1}$) (Fig. 4). This species was identified as a $[Fe^{III}(OOH)(L^1)]^{2+}$ complex (**3**) by high-resolution mass spectrometry (HRMS) (*cf.* Figs.

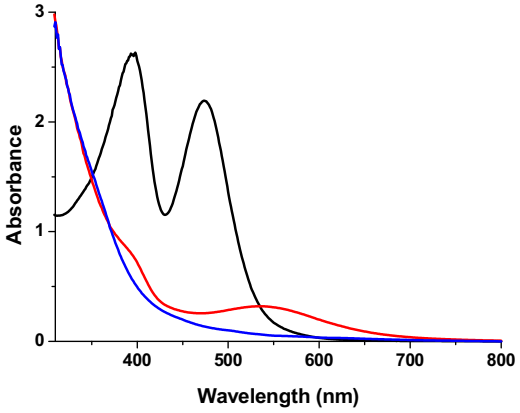

Fig. 4. The UV/Vis spectra of $\mathbf{1}^{OTf}$ (black line), **3** (red line) and decay product of **3** (blue line) in acetonitrile measured at room temperature. (For interpretation of the references to colour in this figure legend, the reader is referred to the web version of this article.)

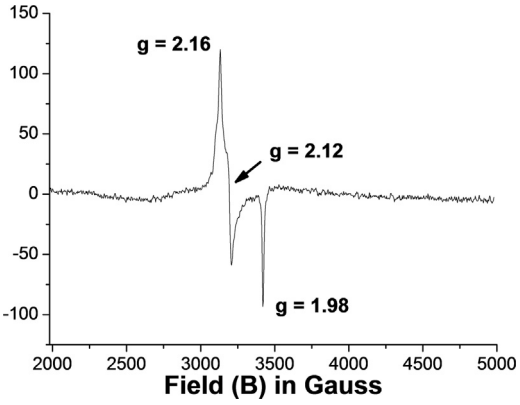

Fig. 5. The X-band EPR spectrum (at 80 K) of a frozen solution of $\mathbf{1}^{OTf} + H_2O_2$ in CH_3CN (after mixing at −20 °C).

S1–S3, Supplementary material). However, the species decomposed during the mass spectrometric measurement to form the corresponding $[Fe^{IV}(O)(L^1)]^{2+}$ species with a prominent mass peak at *m*/*z* 246.0688 (*cf.* Figs. S1–S3, SI). The transient species **3** has a half-life of about 3.7 min at room temperature.

An EPR spectroscopy measurement of complex $\mathbf{1}^{OTf}/H_2O_2$ in CH_3CN also indicated the formation of **3** as a low spin Fe^{III} species, exhibiting g-values at 1.98, 2.12, 2.16 (Fig. 5). These values are very similar to those obtained for a low spin $[Fe^{III}(OOH)(N4Py)]^{2+}$ species (g-values: 1.98, 2.12, 2.17) [19a].

The addition of excess H_2O_2 at room temperature to complex **2** in acetonitrile did not lead to purple colouration, rather a brownish yellow colour appeared (Fig. 6), which could presumably be an Fe(III)-OH species. However, HRMS collected for a cooled (−20 °C) acetonitrile solution containing complex **2** with H_2O_2 showed mass peaks at *m*/*z* 281.0809 and 661.1125, corresponding to the formulations $[Fe^{III}(OOH)(L^2)]^{2+}$ (calc. 281.0822) and $[Fe^{III}(OOH)(L^2)(ClO_4)]^{+}$ (calc. 661.1134) (*cf.* Figs. S4–S6, Supplementary Material). A prominent mass peak at *m*/*z* 272.5826, corresponding to $[Fe^{IV}(O)(L^2)]^{2+}$ (calc. 272.5808), appeared; this ferryl complex might be formed by decomposition of the $[Fe^{III}(OOH)(L^2)]^{2+}$ complex during the measurement.

Formation of $[Fe^{III}(OOH)(L^2)]^{2+}$ was further established by EPR spectroscopy. Complex **2** in CH_3CN together with H_2O_2 (at −20 °C) exhibited EPR signals with g-values 1.98, 2.12, 2.16 (Fig. 7), which could be assigned to a low spin $[Fe^{III}(OOH)(L^2)]^{2+}$ species (*vide supra*).

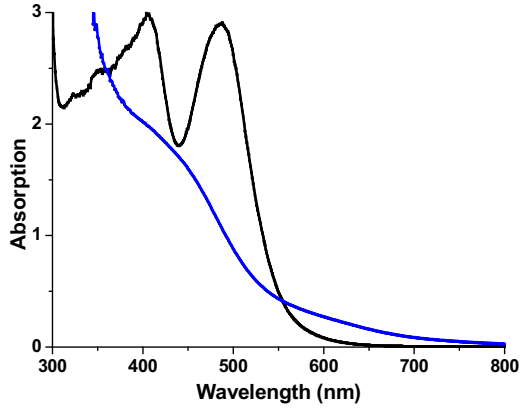

Fig. 6. The UV/Vis spectra of **2** (black line) and $\mathbf{2} + H_2O_2$ (blue line) in acetonitrile measured at room temperature. (For interpretation of the references to colour in this figure legend, the reader is referred to the web version of this article.)

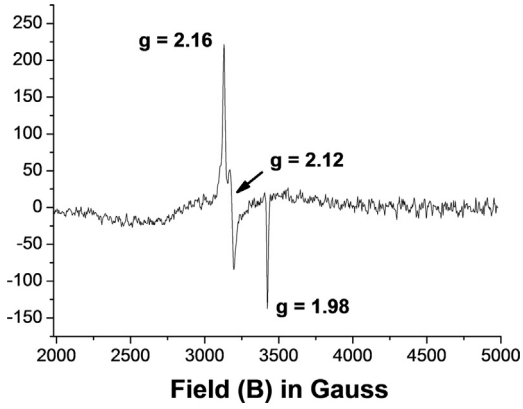

Fig. 7. The X-band EPR spectrum (at 80 K) of a frozen solution of $\mathbf{2} + H_2O_2$ in CH_3CN (after mixing at −20 °C).

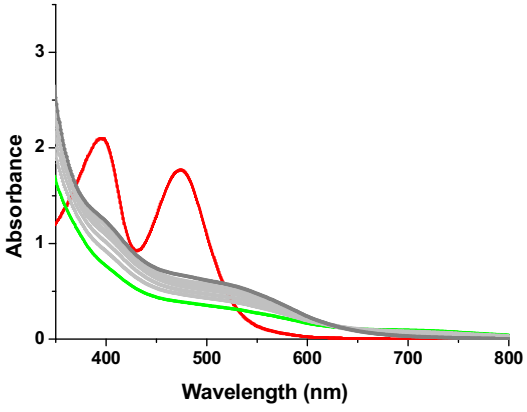

Fig. 8. The UV/Vis spectral change taking place upon addition of mCPBA to 1^{OTf} (red line) in CH_3CN at room temperature. (For interpretation of the references to colour in this figure legend, the reader is referred to the web version of this article.)

On the other hand, the reaction of $\mathbf{1}^{OTf}$ with mCPBA resulted in the formation of a transient $Fe^{IV}(O)$ species, as indicated by UV/Vis spectroscopy and HRMS. The room temperature UV/Vis spectrum of $\mathbf{1}^{OTf}$ with excess mCPBA showed the formation of a transient species with a broad absorbance maximum in the range 720–725 nm (*cf.* Fig. S7, SI). This transient species decayed very rapidly at room temperature to form a new species (Fig. 8) which possibly could be an Fe(III) species.

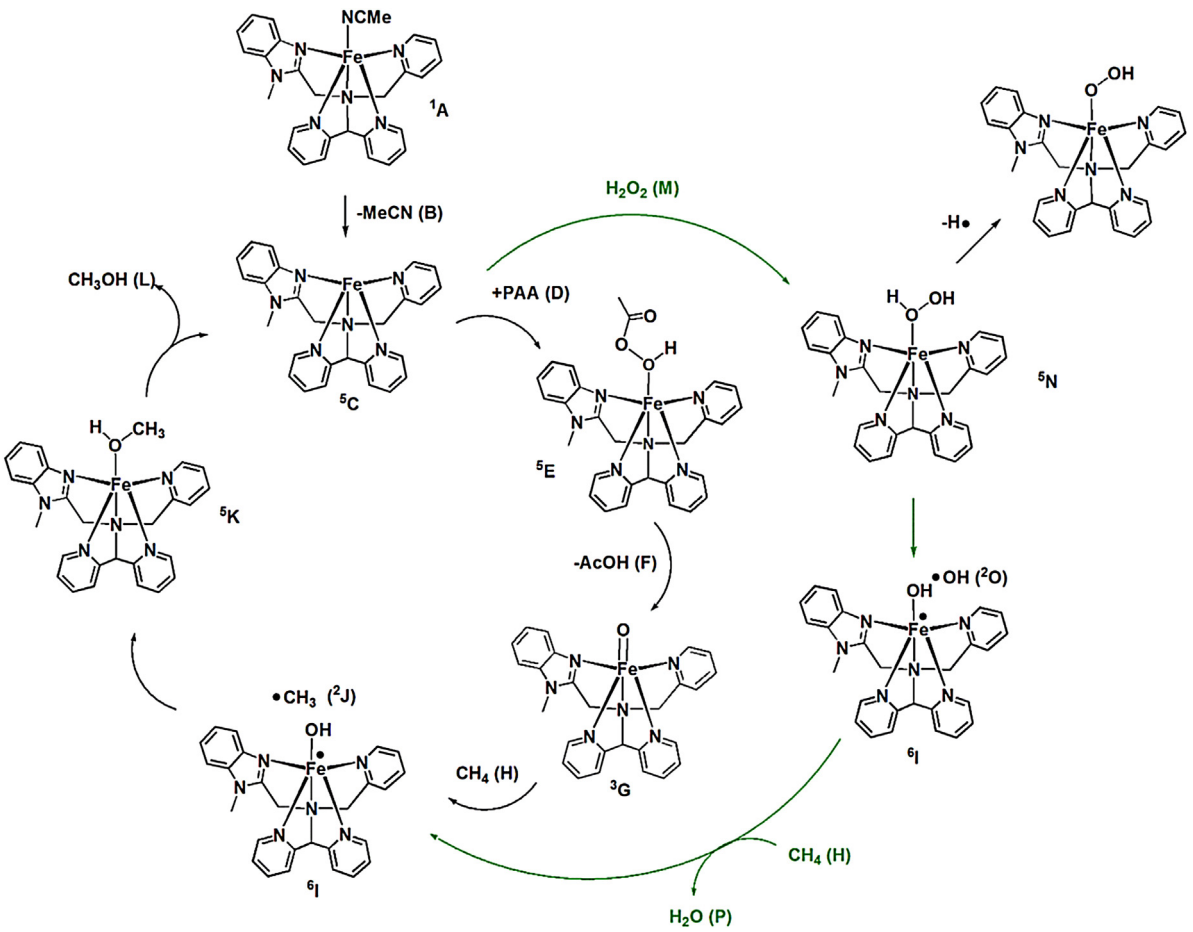

Fig. 9. DFT-computed catalytic cycles for the oxidation of methane (H) to methanol (L) by ^{1}A and the oxidants PAA (D) and H_2O_2 (M). All iron species possess a charge of 2^+.

The HRMS spectrum of $\mathbf{1}^{OTf}$ together with mCPBA (mixed at −20 °C) showed formation of $[Fe^{IV}(O)(L^1)]^{2+}$ as well as $[Fe^{IV}(O)(L^1)(CF_3SO_3)]^+$ (*cf.* Figs. S8–S10, Supplementary Material). The isotopic distribution patterns were found to correspond to the formulations of dicationic $[Fe^{IV}(O)(L^1)]^{2+}$ and monocationic $[Fe^{IV}(O)(L^1)(CF_3SO_3)]^+$. Therefore, the transient species observed in the UV/Vis spectra is most likely $[Fe^{IV}(O)(L^1)]^{2+}$, which decays rapidly at room temperature under the reaction conditions.

4. Computational investigation

The mechanistic pathways involved in the C—H oxidations employing the peracid and H_2O_2 oxidants were computationally evaluated by DFT for compound **1** (^{1}**A**) using methane (**H**) as the hydrocarbon substrate; the latter compound was chosen to simplify the DFT calculations of the oxidation reaction. Fig. 9 shows the computed catalytic cycles starting from the labile MeCN-substituted compound **1** (^{1}**A**).

Species ^{1}**A** has previously been addressed in our recent work on the formation of nonheme Fe(IV)-oxo compounds derived from **1** (^{1}**A**) and PhIO [32]. Dissociation of MeCN (B) from ^{1}**A** generates the unsaturated iron species ^{5}**C**. This process is slightly endergonic with the products lying 8.7 kcal/mol above the starting material. Coordination of the oxidant PAA gives ^{5}**E** which then eliminates AcOH (**F**) to yield the triplet Fe(IV)(oxo) species ^{3}**G** as the ground-state. However, the kinetically active species is the corresponding high spin quintuplet Fe(IV)oxo complex, ^{5}**G**, which lies 2.6 kcal/mol above the ground-state triplet. H-atom abstraction from methane (**H**) by ^{5}**G** occurs in the σ-directed rather than π-directed manifold. The underlying theory behind this two-site reactivity model has been demonstrated by Shaik in related non-heme Fe(IV) species [33]. Successful H-atom transfer produces the geminate radical pair ^{6}**I** and ^{2}**J**, and their collapse affords the MeOH-coordinated compound ^{5}**K**. The release of MeOH (L) liberates the oxidation product and regenerates unsaturated ^{5}**C**, completing the catalytic cycle. The net reaction (**D** + **H** → **F** + **L**) is exergonic at −43.5 kcal/mol.

The catalytic cycle employing H_2O_2 (**M**) proceeds through the initial coordination of M by ^{5}**C**. While the resulting product ^{5}**N** is similar to ^{5}**E**, the fate of the coordinated oxidant is different. Here O—O bond homolysis can yield the geminate radical pair ^{6}**I** and ^{2}**O** and then hydrogen abstraction from methane (**H**) by the hydroxyl radical (^{2}**O**) would yield H_2O (**P**) and the methyl radical (^{2}**J**). At this point, just as in the PAA reaction pathway, the collapse of the resulting radicals, ^{6}**I** and ^{2}**J**, can give ^{5}**K**, which then undergoes loss of MeOH (**L**) and reformation of ^{5}**C**. The net reaction (**H** + **M** → **L** + **P**) is exergonic and comparable to the earlier reaction, liberating −43.8 kcal/mol.

The experimentally observed KIEs using cyclohexane as the substrate are in general agreement with the expected behaviour of the active oxidants computed in the two catalytic cycles. The Fe(IV)(oxo) species ^{5}**G**, which is produced when PAA (**D**) is used as the oxidant, is expected to react more slowly than the hydroxyl radical (^{2}**O**) that results from O—O bond cleavage in ^{5}**N**. Application of the Hammond postulate predicts lower KIE values for C—H/C—D bond activation from the more aggressive hydroxyl radical.

5. Summary and conclusions

The complexes $[Fe^{II}(L^1)(CH_3CN)](ClO_4)_2$ (**1**) and $[Fe^{II}(L^2)(CH_3CN)](ClO_4)_2$ (**2**) are competent catalyst precursors for oxidation of alkanes by hydrogen peroxide and peracids (peracetic acid and *m*-chloroperoxybenzoic acid). Kinetic isotope effect measurements and alcohol/ketone ratios indicate that when H_2O_2 is used as an oxidant, a Fenton-type mechanism takes place, where the metal complex serves to generate hydroxyl radicals that function as the effective oxidants. Formation of low-spin Fe(III)-OOH species from both **1** and **2** have been detected in the H_2O_2-based catalytic system by UV/Vis, mass spectrometry, and EPR spectroscopy and such species may be immediate precursors to hydroxyl radicals, which would be generated by homolytic cleavage of the O—O bond. On the other hand, when the peracids are used as oxidants, relatively high kinetic isotope effects and high C3/C2 selectivity parameters in *cis*-DMCH oxidation are detected, effectively ruling out a Fenton-type mechanism. For these oxidants, we postulate that the catalytic oxidation mechanism involves $[Fe^{IV}(O)(L)]^{2+}$ (L = L^1, L^2) species that react with the substrates. These Fe(IV) oxo complexes have previously been isolated and characterized by reaction of **1** or **2** with iodosyl benzene [32]. The lack of stereoretention that is observed in the oxidation of *cis*-dimethylcyclohexane when peracids are used as the ultimate oxidants (*vide supra*) suggests that the Fe(III)-OH species that are generated in the initial hydrogen atom transfer step are relatively sluggish oxidants, and that the rate of epimerization of the substrate (radical) is faster than the rebound step. It should be noted that theoretical and experimental studies on $[Fe^{IV}(O)(N4Py)]^{2+}$ indicate that the substrate radical generated upon hydrogen atom transfer may dissociate before oxygen rebound (leading to facile epimerization) [34]. Overall, the catalytic reactivities of the Fe(II) complexes follow similar trends (in terms of efficiencies and mechanistic scenarios) to that of $[Fe^{II}(N4Py)(CH_3CN)](ClO_4)_2$ and can be regarded to belong amongst the most efficient nonheme mononuclear iron catalysts.

6. Experimental section

6.1. Materials and methods

All solvents were of at least 99.5% purity and used as received. Reagents were of at least 99% purity and used without any further purification. The reagents and solvents were purchased from Sigma-Aldrich and Fisher chemicals.

UV/vis spectra and all kinetic experiments were performed on a VWR double-beam UV/vis spectrophotometer. The reaction mixture in the case of kinetic experiments and the complex solution in case of spectral scans were placed in a 1 cm quartz cell. The mass spectrometry (ESI) was performed with a Bruker HCT Ultra instrument. The high-resolution mass spectrum (HRMS) was recorded using a Bruker FTICR APEX IV instrument. EPR spectra (X-band, 9.46 GHz) were recorded on a Bruker ECS 106 spectrometer at 80 K using liquid nitrogen. Product analyses were performed on an Agilent Technologies 7820 A gas chromatograph with a 16 sample automatic liquid sampler and flame ionization detector. The products were identified by their GC retention times.

6.2. Syntheses

The Fe(II) complexes, $[Fe^{II}(L^1)(CH_3CN)](ClO_4)_2$ (**1**) and $[Fe^{II}(L^2)(CH_3CN)](ClO_4)_2$ (**2**) were prepared using a literature procedure [32].

6.2.1. Synthesis of $[Fe^{II}(CH_3CN)(L^1)](CF_3SO_3)_2$ (1^{OTf})

A total of 63 mg (0.15 mmol) of ligand $\mathbf{L}^1$ was taken in a vial and dissolved in a minimum amount of acetonitrile. To this solution, 65.4 mg (0.15 mmol) of $[Fe(CH_3CN)_2(CF_3SO_3)_2]$ in acetonitrile was added under stirring at room temperature under nitrogen atmosphere. After stirring for about 30 min, the reaction mixture was placed into an ethyl acetate bath and stored overnight. The precipitate was collected by filtration, washed with ethyl acetate, dried under vacuum and obtained as red solid. Yield: 87 mg (71%). ESI–MS (in CH_3CN): *m*/*z* 238.1 $[Fe^{II}(L^1)]^{2+}$ (*z* = 2) calc. 238.1, 625.1 $[Fe^{II}(L^1)(CF_3SO_3)]^+$ (*z* = 1) calc. 625.1. Anal.Cald (%): C 44.18, H 3.34, N 12.02; Found (%): C 43.94, H 3.77, N 11.91.

6.3. Reaction conditions for catalysis

In a typical reaction, 2 ml of 100 mM (200 μmol) H_2O_2 (diluted from 35% H_2O_2 aqueous solution) or 2 ml of 100 mM (200 μmol) PAA/mCPBA solution in CH_3CN was delivered by syringe pump in air or under nitrogen to a stirred solution of catalyst, i.e. complex **1** (2 μmol), and the substrate (2000 μmol) inside a vial. The final concentrations of the reagents were ~0.7 mM iron catalyst, ~70 mM oxidant, and ~700 mM substrate. After syringe pump addition, a known amount (500 μl) of biphenyl solution was added as an internal standard. The iron complex was removed by passing the reaction mixture through a small silica column followed by elution with ethyl acetate. Finally, the solutions were subjected to GC analysis. The organic products were identified, and their yields were determined by comparison with authentic compounds.

The kinetic isotope effect (KIE) in the reactions were determined from an equimolar mixture of cyclohexane and cyclohexane-d_{12} for those reactions performed under nitrogen atmosphere.

6.4. Computational details and modeling

All DFT calculations were carried out with the Gaussian 09 package of programs [35], using the B3LYP hybrid functional. This functional is comprised of Becke's three-parameter hybrid exchange functional (B3) [36] and the correlation functional of Lee, Yang, and Parr (LYP) [37]. The iron atom was described with the Stuttgart-Dresden effective core potential and valence basis set [38], and the 6–31G(d') basis set [39] was employed for all remaining atoms. The iron-based structures were optimized as a function of the spin state and only the lowest energy species are shown in the catalytic cycle (Fig. 9). Here the superscript number for each species represents the preferred multiplicity. For those molecules with a singlet ground-state (**B**, **D**, **F**, **H**, **L**, **M**, and **P**), the multiplicity is assumed to be one (2S + 1 = 1) and no multiplicity designation is specified in the labeling scheme of the catalytic cycle.

All reported geometries were fully optimized, and evaluation of the analytical Hessian showed each stationary point to be an energy minimum (no negative eigenvalues). Unscaled vibrational frequencies derived from the analytical Hessian were used to calculate the zero-point and thermal corrections to the electronic energies. The resulting free energies are reported in kcal/mol relative to the specified standard. Standard state corrections were applied to all species to convert concentrations from 1 atm to 1 M according to the treatise of Cramer [40]. The geometry-optimized structures have been drawn with the *JIMP*2 molecular visualization and manipulation program [41].

Acknowledgments

This research has been carried out within the framework of the International Research Training Group *Metal Sites in Biomolecules: Structures, Regulation, and Mechanisms* (www.biometals.eu) and has also been supported by COST Action CM1003. M.M thanks the European Union for an Erasmus Mundus fellowship. MGR thanks the Robert A. Welch Foundation (grant B-1093) and the Wenner-Gren Foundation for financial support and acknowledges

computational resources through UNT's High-Performance Computing Services and CASCAM.

Appendix A. Supplementary data

Supplementary data associated with this article can be found, in the online version, at http://dx.doi.org/10.1016/j.molcata.2016.10.010.

References

[1] (a) T. Newhouse, P.S. Baran, Angew. Chem. Int. Ed. 50 (2011) 3362–3374;
(b) L. McMurray, F. O'Hara, M.J. Gaunt, Chem. Soc. Rev. 40 (2011) 1885–1898;
(c) M. Bordeaux, A. Galarneau, J. Drone, Angew. Chem. Int. Ed. 51 (2012) 10712–10723.
[2] (a) C-H and C-X Bond Functionalization, X. Ribas (Ed.) Royal Society of Chemistry, Cambridge, 2013;
(b) Biomimetic Oxidations Catalyzed by Transition Metal Complexes, B. Meunier (Ed.), Imperial College Press, London, 2000.
[3] A.E. Shilov, G.B. Shul'pin, Chem. Rev. 97 (1997) 2879–2932.
[4] M. Costas, M.P. Mehn, M.P. Jensen, L. Que Jr., Chem. Rev. 104 (2004) 939–986.
[5] S.V. Kryatov, E.V. Rybak-Akimova, S. Schindler, Chem. Rev. 105 (2005) 2175–2226.
[6] M. Merkx, D.A. Kopp, M.H. Sazinsky, J.L. Blazyk, J. Muller, S.J. Lippard, Angew. Chem. Int. Ed. 40 (2001) 2782–2807.
[7] M.M. Abu-Omar, A. Loaiza, N. Hontzeas, Chem. Rev. 105 (2005) 2227–2252.
[8] L. Que Jr., W.B. Tolman, Nature 455 (2008) 333–340.
[9] M. Costas, K. Chen, L. Que Jr., Coord. Chem. Rev. 200–202 (2000) 517–544.
[10] (a) G.J.P. Britovsek, J. England, A.J.P. White, Inorg. Chem. 44 (2005) 8125–8134;
(b) J. England, G.J.P. Britovsek, N. Rabadia, A.J.P. White, Inorg. Chem. 46 (2007) 3752–3767;
(c) J. England, R. Gondhia, L. Bigorra-Lopez, A.R. Petersen, A.J.P. White, G.J.P. Britovsek, Dalton Trans. (2009) 5319–5334.
[11] K.P. Bryliakov, E.P. Talsi, Coord. Chem. Rev. 276 (2014) 73–96.
[12] (a) C. Kim, K. Chen, J. Kim, L. Que Jr., J. Am. Chem. Soc. 119 (1997) 5964–5965;
(b) J. Kim, R.G. Harrison, C. Kim, L. Que Jr., J. Am. Chem. Soc. 118 (1996) 4373–4379.
[13] (a) K. Chen, L. Que Jr., Chem. Commun. (1999) 1375–1376;
(b) K. Chen, L. Que Jr., J. Am. Chem. Soc. 123 (2001) 6327–6337.
[14] M.S. Chen, M.C. White, Science 318 (2007) 783–787.
[15] (a) A. Company, L. Gomez, M. Guell, X. Ribas, J.M. Luis, L. Que Jr., M. Costas, J. Am. Chem. Soc. 129 (2007) 15766–15767;
(b) A. Company, L. Gomez, X. Fontrodona, X. Ribas, M. Costas, Chem. Eur. J. 14 (2008) 5727–5731.
[16] M. Mitra, J. Lloret-Fillol, M. Haukka, M. Costas, E. Nordlander, Chem. Commun. 50 (2014) 1410–1412.
[17] (a) J. Stubbe, J.W. Kozarich, Chem. Rev. 87 (1987) 1107–1136;
(b) S.M. Hecht, Acc. Chem. Res. 19 (1986) 383–391.
[18] (a) J.W. Sam, X.-J. Tang, J. Perisach, J. Am. Chem. Soc. 116 (1994) 5250–5256;
(b) T.E. Westre, K.E. Loeb, J.M. Zaleski, B. Hedman, K.O. Hodgson, E.I. Solomon, J. Am. Chem. Soc. 117 (1995) 1309–1313;
(c) R.M. Burger, T.A. Kent, S.B. Howitz, E. Munck, J. Perisach, J. Biol. Chem. 258 (1983) 1559–1564.
[19] (a) M. Lubben, A. Meetsma, E.C. Wilkinson, B.L. Feringa, L. Que Jr., Angew. Chem. Int. Ed. 34 (1995) 1512–1514;
(b) G. Roelfes, M. Lubben, S.W. Leppard, E.P. Schudde, R.M. Hermant, R. Hage, E.C. Wilkinson, L. Que Jr., B.L. Feringa, J. Mol. Catal. A 117 (1997) 223–227.
[20] G. Roelfes, M. Lubben, R. Hage, L. Que Jr., B.L. Feringa, Chem. Eur. J. 6 (2000) 2152–2159.
[21] V. Balland, D. Mathieu, N. Pons-Y-Moll, J.F. Bartoli, F. Banse, P. Battiioni, J.-J. Girerd, D. Mansuy, J. Mol. Catal. A: Chem. 215 (2004) 81–87.
[22] I. Bernal, I.M. Jensen, K.B. Jensen, C.J. McKenzie, H. Toftlund, J.-P. Tuchagues, J. Chem. Soc. Dalton Trans. (1995) 3667–3675.
[23] G. Roelfes, V. Vrajmasu, K. Chen, R.Y.N. Ho, J.U. Rohde, C. Zondervan, R.M. laCrois, E.P. Schudde, M. Lutz, A.L. Spek, R. Hage, B.L. Feringa, E. Munck, L. Que Jr., Inorg. Chem. 42 (2003) 2639–2653.
[24] A.K. Patra, M.M. Olmstead, P.K. Mascharak, Inorg. Chem. 41 (2002) 5403–5409.
[25] A. Grohmann, Adv. Inorg. Chem. 56 (2004) 179–202.
[26] M. You, M.S. Seo, K.M. Kim, W. Nam, J. Kim, Bull. Korean Chem. Soc. 27 (2006) 1140–1145.
[27] T.A. van den Berg, J.W. de Boer, W.R. Browne, G. Roelfes, B.L. Feringa, Chem. Commun. (*2004*) 2550–2551.
[28] G. Roelfes, M. Lubben, K. Chen, R.Y.N. Ho, A. Meetsma, S. Genseberger, R.M. Hermant, R. Hage, S.K. Mandal, V.G. Young Jr., Y. Zang, H. Kooijman, A.L. Spek, L. Que Jr., B.L. Feringa, Inorg. Chem. 38 (1999) 1929–1936.
[29] (a) J. Kaizer, E.J. Klinker, N.Y. Oh, J.U. Rohde, W.J. Song, A. Stubna, J. Kim, E. Munck, W. Nam, L. Que Jr., J. Am. Chem. Soc. 126 (2004) 472–473;
(b) E.J. Klinker, J. Kaizer, W.W. Brennessel, N.L. Woodrum, C.J. Cramer, L. Que Jr., Angew. Chem. Int. Ed. 44 (2005) 3690–3694.
[30] N. Lehnert, F. Neese, R.Y.N. Ho, L. Que Jr., E. Solomon, J. Am. Chem. Soc. 124 (2002) 10810–10822.
[31] D. Kumar, H. Hirao, L. Que Jr., S. Shaik, J. Am. Chem. Soc. 127 (2005) 8026–8027.
[32] M. Mitra, H. Nimir, S. Demeshko, S.S. Bhat, S.O. Malinkin, M. Haukka, J. Lloret-Fillol, G.C. Lisensky, M. Meyer, A. Shteinman, W.R. Browne, D.A. Hrovat, M.G. Richmond, M. Costas, E. Nordlander, Inorg. Chem. 54 (2015) 7152–7164.
[33] D. Usharani, D. Janardanan, C. Li, S. Shaik, Acc. Chem. Res. 46 (2013) 471–482, and references therein.
[34] K.-B. Cho, X. Wu, Y.-M. Lee, Y.H. Kwon, S. Shaik, W. Nam, J. Am. Chem. Soc. 134 (2012) 20222–20225.
[35] M.J. Frisch, et al., Gaussian 09, Revision E.01, Gaussian, Inc., Wallingford, CT USA, 2009.
[36] A.D. Becke, J. Chem. Phys. 98 (1993) 5648–5652.
[37] C. Lee, W. Yang, R.G. Parr, Phys. Rev. B 37 (1988) 785–789.
[38] (a) M. Dolg, U. Wedig, H. Stoll, H. Preuss, J. Chem. Phys. 86 (1987) 866–872;
(b) S.P. Walch, C.W. Bauschlicher, J. Chem. Phys. 78 (1983) 4597–4605.
[39] (a) G.A. Petersson, A. Bennett, T.G. Tensfeldt, M.A. Al-Laham, W.A. Shirley, J. Mantzaris, J. Chem. Phys. 89 (1988) 2193–2218;
(b) G.A. Petersson, M.A. Al-Laham, J. Chem. Phys. 94 (1991) 6081–6090.
[40] C.J. Cramer, Essentials of Computational Chemistry, 2nd ed., Wiley, Chichester, UK, 2004.
[41] (a) M.B. Hall, R.F. Fenske, Inorg. Chem. 11 (1972) 768–775;
(b) A free program for the visualization and manipulation of molecules, JIMP2, version 0.091, J. Manson, C.E. Webster, M.B. Hall, Texas A&M University, College Station, TX, 2006: http://www.chem.tamu.edu/jimp2/index.html.